Temperature-dependent spectral emissivity of microstructured silicon

Elissa Akiki, Georges Hamaoui, Armande Herve, Yang An, Frédéric Marty, Jianping Zou, Arthur Fortin, Tarik Bourouina, Philippe Basset, Agnès Delmas, et al.

Temperature-Dependent Spectral Emissivity of Microstructured Silicon

Elissa Akiki[1+], Georges Hamaoui[1+*], Armande Herve[1+], Yang An[2], Frédéric Marty[1], Jianping Zou[3], Arthur Fortin[1], Tarik Bourouina[1,3], Philippe Basset[1], Agnès Delmas[4], Elyes Nefzaoui[1*]

[1]ESYCOM lab, Univ Gustave Eiffel, CNRS, ESYCOM, F-77454 Marne-la-Vallée, France

[2]CIOMP, Chinese Academy of Sciences, Changchun, China

[3]CINTRA, IRL 3288 CNRS-NTU-THALES, Nanyang Technological University, Singapore 637553, Singapore

[4]CETHIL, UMR 5008 CNRS, INSA Lyon, UCBL, Université de Lyon, Villeurbanne, France

[*]georges.hamaoui@univ-eiffel.fr

[*]elyes.nefzaoui@univ-eiffel.fr

[+]Equal contribution

This work presents an experimental investigation of the temperature dependence of spectral and total emissivity of microstructured highly doped silicon, a class of Black Silicon (BSi) surfaces, which behaves as an ultra-broadband and ultra-black behavior, nearly a perfect blackbody up to a wavelength of 10 µm. We make a comparison with a flat surface of similar silicon taken as a reference. Direct infrared (IR) emissivity measurements were performed under normal incidence across 2–20 µm spectral range and at temperatures between 100 °C and 350 °C, using a newly developed experimental setup. While previous studies have demonstrated the excellent absorptivity of BSi at room temperature, our results confirm that BSi maintains near-unity emissivity up to a wavelength of 10 µm even at high temperatures. Notably, the total hemispherical emissivity is found to increase slightly from ~0.95 at 150 °C up to ~0.98 at 350 °C. These values significantly exceed by far those of the flat Si reference samples. The results are further compared with absorptivity measurements at room temperature obtained from FTIR spectroscopy and with literature data. This study provides a comprehensive temperature resolved and spectrally resolved emissivity properties for highly doped BSi, establishing its suitability for advanced thermal applications such as thermophotovoltaic emitters, thermal infrared light sources, and radiative cooling.

Keywords: Black Silicon (BSi), Spectral emissivity, Infrared radiative properties, Thermal metamaterials, Direct emissivity measurement

I. Introduction

Meta-materials for thermal radiation control and conversion have been a very active field of research during the past decade in relation with several applications such as thermoelectrics, photovoltaics, and thermophotovoltaics (TPV), as well as in managing the thermal properties of electronic devices, thermal rectification, and radiative cooling for extensive thermal regulation [1–5]. Such meta-materials are often made of ordered structures such as 1D or 2D periodic structures, photonic crystals, multilayers, resonant cavities, and surface gratings among others. In this contribution, we focus on randomly sub micro-structured silicon surfaces alternatively known as black silicon (BSi). BSi [6–8], has attracted significant attention due to its ease of fabrication, system integration compatibility, and scalable cost-effectiveness qualities that leverage silicon's numerous use in the microelectronics industry [9, 10]. BSi, with its micro- and nanostructured surface, has a primary function of minimizing reflectivity owing the smooth transition of the effective refraction index at the interface between the incidence medium and the silicon volume. Consequently, depending on the doping concentration, the silicon volume can fully absorb the trapped incident light. This synergetic action of surface structuration and doping eventually ensures extremely high absorptivity and emissivity extending to the mid-infrared spectral range [11, 12].

In previous work, we have extensively investigated the optical properties of BSi fabricated using cryogenic deep reactive ion etching (Cryo-DRIE) [13]. Our latest studies have focused on how surface morphology, doping level, doping profile [11, 12], as well as surface functionalization [14], influence the material's radiative behavior. Both modeling and experimental work have demonstrated that increasing the doping concentration enhances absorptance across the near- to far-infrared spectrum, while optimizing the aspect ratio, especially through deep conical nanostructures, improves isotropic absorption [11, 12, 15, 16]. These parameters offer multiple degrees of freedom to tailor the spectral emissivity or absorptivity to specific application needs.

We have also explored the potential of BSi in various thermal radiation harvesting applications, such as solar steam generation, radiative cooling, and dew water collection, where the material typically operates at or near room temperature [4, 5, 17–19]. However, in applications like TPV selective emitters or infrared radiation sources for spectroscopy, the material is required to perform at elevated temperatures. This shift in operational conditions highlights the need for experimental characterization of BSi's emissivity at higher temperatures to evaluate its full potential in these advanced applications.

Emissivity is the key thermal property that governs heat transfer in these applications. It describes a material's ability to emit thermal radiation relative to an ideal blackbody (BB). Emissivity is typically determined using either direct or indirect measurement methods [20]. The indirect method involves projecting a radiation beam onto a sample and measuring both reflectivity (ρ) and transmissivity (τ) to deduce absorptivity (α). Then using Kirchhoff's law, which states that spectral directional absorptivity (α) and emissivity (ϵ) are equivalent for a material at thermal equilibrium, ϵ is calculated [21]. Conversely, the direct method calculates emissivity based on the ratio of thermal radiation emitted by the sample to that from a BB reference source under the same conditions.

The choice between these methods largely depends on the experimental setup and specific application needs. An advantage of the indirect method is that it enables measurements of α at lower temperatures, as it does not rely on measuring the thermal power emitted by the sample itself. The direct method is typically chosen for high-temperature materials, where the signal-to-noise ratio is more favorable, enabling a clearer differentiation between the sample's emitted radiation and that reflected from ambient conditions [22, 23]. However, direct measurements near ambient temperatures remain challenging due to significant noise at wavelengths below 4 μm caused by weak signal energy [24, 25].

Accurate evaluation of the emissivity of flat silicon and BSi under realistic operating conditions requires direct measurements at elevated temperatures. However, many previous studies on silicon-based meta-materials have been restricted to narrow temperature and spectral ranges along doping levels, limiting their relevance for real-world applications [11, 26–29].

Previous work in the field includes the transmission spectra measurements by Macfarlane *et al.*, who studied flat silicon in the 0.95–1.35 μm range over temperatures from -272.8 to 142°C [30]. Similarly, Sato investigated the spectral emissivity of lightly doped n-type flat silicon (resistivity of 15 Ω·cm), covering 0.4–15 μm wavelengths and temperatures between 270 and 520 °C [31]. Sato's results were then used by P. J. Timans, who measured flat silicon absorption in the 1.1–1.6 μm range for temperatures up to 800 °C [32]. Meanwhile H. Rogne used isothermal electron beam heating with in situ optical measurements to study the spectral emissivity of lightly doped flat silicon between 345–723 °C and 1–9 μm wavelengths [33]. Further studies revealed absorption/emissivity temperature dependence at specific IR wavelengths (1.152, 1.3, 1.55, 1.7, 3.4, and 10.6 μm) [34–36].

A broader parametric exploration was conducted by Ravindra *et al.*, who combined experimental and simulation approaches to assess emissivity as a function of wavelength for highly doped flat Si (resistivity of 0.02-0.005 Ω·cm), over 1–12 μm and 183–947 °C [29]. In a separate study, Ravindra *et al.* [37] also

investigated highly-doped flat Si surfaces coated with SiO_2 and Si_3N_4 layers using a spectral emissometer covering 0.8–20 μm and 20–1000 °C. They observed that emissivity initially increases with oxide thickness, then decreases, with the peak thickness remaining temperature-independent for a given wavelength. Later, Marcio Constancio Jr. *et al.* estimated temperature-dependent effective emissivity of lightly doped Si (resistivity of 4360 Ω·cm) from its cooling curve at -191°C [38].

Focusing specifically on microstructured silicon, P. G. Maloney *et al.* measured IR transmittance and hemispherical-directional reflectance from 2.5–25 μm for highly doped BSi (resistivity of 0.005 Ω·cm) manufactured using femtosecond laser irradiation in SF_6 or Cl_2, calculating spectral emissivity from a 200 °C IR source [26]. The resulting microstructures featured spike heights of up to 40 μm. Their results showed that BSi already outperforms low-doped flat Si in emissivity at 200 °C, with maximum values of nearly 0.9 dropping to 0.73 beyond 10 μm. Furthermore, Feng *et al.* investigated another low-doped BSi type produced also via femtosecond laser irradiation in SF_6. With spike heights of 8 μm, they measured spectral emissivity from 2.5–25 μm between 100 °C and 400 °C. Their results showed that BSi maintains an emissivity close to 0.96 at 100 °C, slightly decreasing beyond 8 μm but remaining above 0.9 across along most of the measured spectral range [27].

In this work, we experimentally investigate the temperature dependence of the spectral emissivity of highly-doped BSi fabricated using Cryo-DRIE [13], in the 100–350 °C range and over wavelengths from 2 to 20 μm. To this end, we developed a dedicated experimental setup capable of performing direct spectral normal emissivity measurements from room temperature up to 600 °C, across a broad spectral range from 2 to 20 μm. While several previous studies have addressed the emissivity of silicon-based metamaterials, the impacts of surface morphology (related to fabrication methods) and doping levels on the radiative properties of BSi remains insufficiently explored particularly at elevated temperatures. This work aims to fill that gap by providing direct, temperature-resolved and spectrally resolved emissivity data for both microstructured and flat silicon, contributing to a better understanding of their potential for high-temperature radiative applications.

II. Materials and methods

A. Black Silicon fabrication

For this study, Cryo-DRIE was used for the fabrication of BSi. The process uses a SF_6/O_2 chemistry at a temperature of -110°C where SF_6 is the etching gas and O_2 is used as a catalyst for the passivation of the etched walls. High aspect ratio structures are thus formed without the use of photolithography masks [16].

Adjusting etching/passivation times optimizes topography. Hence, the process parameters were chosen based on best practices established in the literature [11, 12, 17] to achieve height and lateral dimensions of 5 µm and 0.3 µm, respectively. The fixed parameters are the source power of 1000 W, the pressure of 2 Pa and the bias voltage of 10 V.

Highly doped (100)-oriented single-crystalline silicon substrate (4", 0.001 Ω·cm, ~5×10^{19} cm^{-3} N-type) were used to suppress transmission (τ) of infrared radiation throughout the sample. An example of the resulting microstructured surface is shown in Figure 1-a.

B. Reference Blackbody fabrication

Accurate direct emissivity measurements require a suitable blackbody (BB) reference source, chosen based on temperature range, spectral coverage, and integration flexibility. Commercial cavity BB sources often demand complex setups, especially at low to intermediate temperatures because of low signal to noise ratios. As an alternative, high-emissivity materials offer easier integration and reduced measurement errors due to their ease of integration. Indeed, they can be adapted and integrated in various setups ensuring identical geometry and optical path when compared to the samples under study. In this work, we fabricated homemade BB reference using 1000 µm-tall vertically aligned carbon nanotubes (VACNTs) grown by CVD. Their excellent emissive properties stem from both the intrinsic optical behavior of CNTs and their light-trapping morphology [39]. Additionally, they have been successfully used in previous studies [40, 41]. The VACNTs CVD process was performed on a silicon substrate, and it involves a preliminary formation of iron oxide nanocluster as the seed for CNT growth on a low-doped Si substrate (resistivity of 1–20 Ω·cm) [42]. A SEM example of the resulting CNT sample is shown in Figure 1-b.

(a) **(b)**

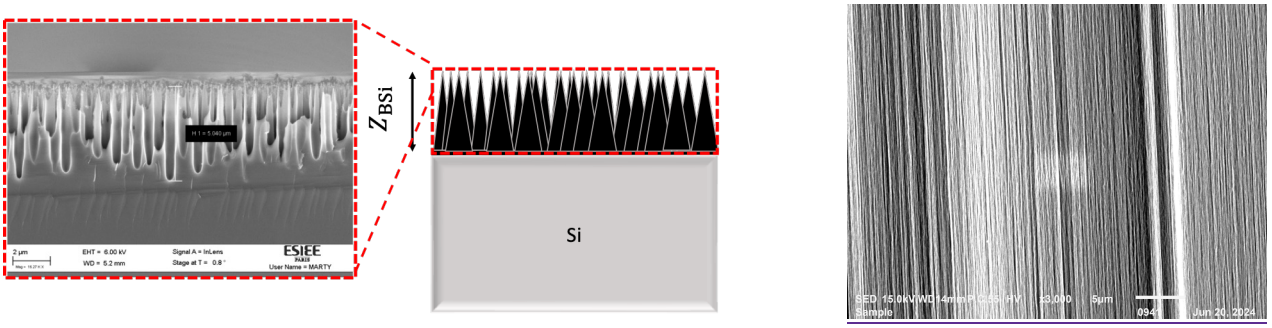

Figure 1 : **(a)** Schematic representation of a microstructured silicon surface along with a cross-sectional SEM image. **(b)** Cross-sectional SEM image of the BB reference CNT sample.

To further validate the suitability of our CNT-based sample as a blackbody reference, we performed additional measurements of both reflectance and transmittance using FTIR spectroscopy (see Figure S1 in the Supplementary Information). These measurements confirm that the transmittance of the vertically aligned CNT layer is negligible ($\tau \approx 0$) across the entire spectral range of 2–20 μm, consistent with the expected behavior of thick, densely packed VACNTs. The reflectance, ρ, was measured to be below 2%, resulting in an absorptivity exceeding 0.98, in agreement with previous reports [39–41]. Furthermore, we evaluated the angular dependence of the CNT absorptivity, α, and confirmed that it remains high and spectrally flat even at oblique incidence (Figure S2), supporting the assumption of near-ideal blackbody behavior. In addition, these CNT-based samples exhibit spectrally flat, broadband absorption ($\alpha \approx 0.98$) up to 20 μm (Figure 3) and remain stable up to 350 °C. These results justify the use of the CNT sample as a reliable reference for our direct emissivity measurements.

Three samples were studied in this work: (i) highly doped (HD) BSi with a resistivity of 0.001 Ω·cm and a nanostructure height of approximately 5 μm, (ii) highly doped (HD) flat silicon Si with the same resistivity of 0.001 Ω·cm, and (iii) a BB reference sample consisting of a vertically aligned CNT layer, 1000 μm tall, grown on a low-doped (LD) silicon substrate with a resistivity ranging from 1 to 20 Ω·cm.

C. Direct emissivity measurement setup

The experimental setup developed in this study is based on a Fourier-transform infrared (FTIR) spectrometer (PerkinElmer Spectrum 400) equipped with a deuterated triglycine sulfate (DTGS) detector operating at room temperature and a KBr beam splitter, enabling spectral coverage from 2 to 20 μm. Each spectrum is obtained by averaging 10 scans to improve signal reliability with a resolution of 4 cm^{-1}. Samples are heated using a vertical heating stage (PIKE Technologies S-100R), which offers precise temperature control up to 600 °C under primary vacuum conditions. The stage features a dual-layer water-cooling system that ensures accurate surface temperature regulation and minimizes convective effects. The heating stage is equipped with a KBr window, which are transparent in the mid-infrared range (2–20 μm) and thus do not significantly affect the measured spectral emissivity within our range of interest. Importantly, all measurements, sample and CNT blackbody reference, were conducted under identical conditions using the same 20 mm stage aperture and through the same window path, ensuring that any influence from the window is effectively canceled out when computing the sample emissivity relative to the reference. The key feature of this setup is that the reference is positioned in the same location as the sample, ensuring that the optical path of the radiation from the BB exactly matches that of the sample measurement.

To improve measurement accuracy, the aperture of the diaphragm (Thorlabs ID50Z/M - Mounted Zero-Aperture Iris) was set to 30 mm and positioned between the sample and the collection optics (off-axis parabolic mirror, Thorlabs MPD269-G01, with a reflected focal length of 152.4 mm), effectively reducing background radiation and enhancing the signal-to-noise ratio. All optical components are enclosed within a blackout chamber with near-maximum mid-infrared absorptivity, effectively minimizing stray reflections and emulating blackbody behavior within the measurement environment. A top view schematic of the experimental setup developed in this study is shown in Figure 2. The red doted beam represents the infrared emission of the BB measured by the FTIR spectrometer.

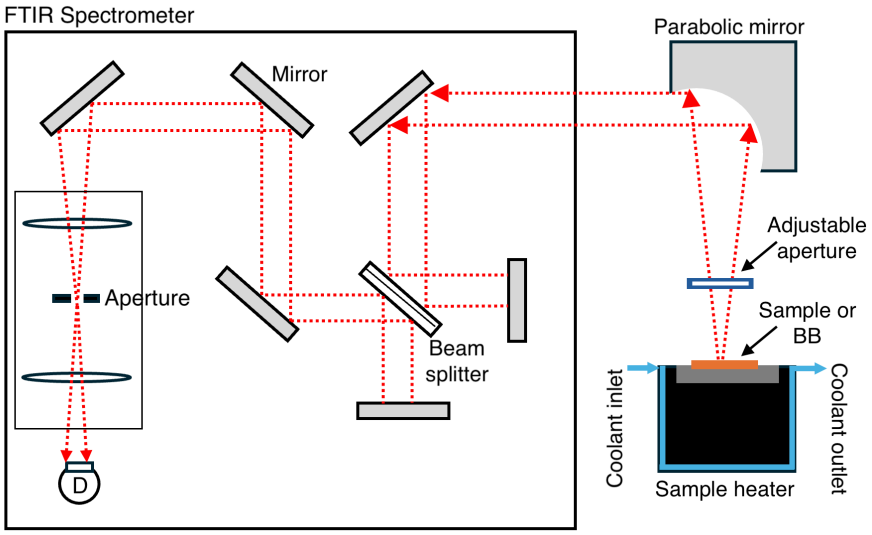

Figure 2 : Direct spectral normal emissivity measurements setup developed and used in this work.

The measured emissivity was compared to absorptivity values obtained at room temperature using FTIR spectroscopy (PerkinElmer Spectrum 3 equipped with a PIKE Technologies 10SPEC and an integrating IR sphere), where the spectral directional absorptivity $\alpha(\lambda)$ was calculated as $\alpha(\lambda) = 1 - \rho^{\cap}(\lambda) - \tau^{\cap}(\lambda)$ with $\rho^{\cap}(\lambda)$ and $\tau^{\cap}(\lambda)$ are respectively the spectral hemispherical reflectivity and transmittivity. According to Kirchhoff's law, spectral emissivity $\epsilon(\lambda)$ is equal to spectral absorptivity $\alpha(\lambda)$ at thermal equilibrium for each wavelength and incidence angle. Therefore, in this study, we use the notation $\alpha(\lambda)$ for the indirect measurements and $\epsilon(\lambda, T)$ for the direct high-temperature measurements, to reflect the different experimental methods and conditions. The labels "absorptivity" and "emissivity" simply refer to the measurement technique (indirect vs. direct) and temperature (room temperature vs. elevated temperatures), not to distinct physical properties.

A theoretical calculation of the spectral absorptivity of silicon with a resistivity of 0.001 Ω·cm was also made in order to compare and validate our measurements. This approach, detailed in the work of Sarkar

et al. [12], is based on the Drude model, with additional adjustments to derive absorptivity from the imaginary part of the refractive index.

D. Calibration and emissivity calculations

Emissivity is the ratio of the spectral and directional radiative intensity $L_s(\lambda, \theta, T_s)$ emitted by a sample at a given temperature T_s, to the spectral intensity $L_{BB}(\lambda, T_s)$ of a blackbody at the same temperature, as given by Planck's law, as

$$\epsilon(\lambda, \theta, T_s) = \frac{L_s(\lambda, \theta, T_s)}{L_{BB}(\lambda, T_s)} \quad (1)$$

By definition, emissivity ranges from 0 to 1. We consider normal incidence ($\theta = 0$) in the first place.

The main challenge of the direct method is to distinguish the contribution of the sample in the effective spectral intensity. The raw spectral signal of the BB resulting from a FTIR measurement is linked to the spectral intensity $L(\lambda, T_{BB})$, the calibration function $R(\lambda)$ and the background signal $S_{bg}(\lambda)$ can be written as follows:

$$S_{BB}(\lambda, T_{BB}) = R(\lambda)\epsilon_{BB}(\lambda)L_{BB}(\lambda, T_{BB}) + S_{bg}(\lambda) \quad (2)$$

where $S_{BB}(\lambda, T_{BB})$ is the raw signal of the BB at a temperature T_{BB}, $\epsilon_{BB}(\lambda)$ is the emissivity of the BB (assumed to be equal to the absorptivity $\alpha(\lambda)$), $L_{BB}(\lambda, T_{BB})$ is the Planck's law at the same temperature and $S_{bg}(\lambda)$ is the background signal. The measured effective spectral intensity of the sample is composed of that emitted by the sample, ambient radiation reflected by the sample and the background radiation. Hence, the sample spectral signal can be expressed as

$$S_s(\lambda, T_s) = R(\lambda)[\epsilon_s(\lambda, T_s)L_s(\lambda, T_s) + \rho_s(\lambda, T_{sur})\epsilon_{sur}(\lambda, T_{sur})L_{sur}(\lambda, T_{sur})] + S_{bg}(\lambda) \quad (3)$$

with $S_s(\lambda, T_s)$ the raw signal of the sample at T_s and measured by the FTIR, $\epsilon_s(\lambda, T_s)$ the emissivity of the sample, $L_s(\lambda, T_s)$ Planck's law at the same temperature, $\rho_s(\lambda, T_{sur})$ the specular reflectivity of the sample (measured by the indirect method at room temperature), $\epsilon_{sur}(\lambda, T_{sur})$ and $L_{sur}(\lambda, T_{sur})$ the emissivity and Planck's law at the temperature of the surrounding background, respectively, and $S_{bg}(\lambda)$ the background signal. In this study, the experimental setup is enclosed in a black chamber which is assumed to be a blackbody with $\epsilon_{sur} = 1$.

Additionally, we perform measurements on the BB at two different temperatures to extract $R(\lambda)$ and $S_{bg}(\lambda)$. Subtracting Eq. (2) for the two measurements at $T_{ref\,1}$ and $T_{ref\,2}$ leads to the calibration function $R(\lambda)$ given by :

$$R(\lambda) = \frac{S_{BB}(\lambda, T_{ref\,1}) - S_{BB}(\lambda, T_{ref\,2})}{\epsilon_{BB}(\lambda)\left[L_{BB}(\lambda, T_{ref\,1}) - L_{BB}(\lambda, T_{ref\,2})\right]} \quad (4)$$

By grouping equations (2) and (3), one can obtain the expression of the spectral emissivity of the heated sample as

$$\epsilon_s(\lambda, T_s) = \frac{S_s(\lambda, T_s) - S_{BB}(\lambda, T_{BB}) + R(\lambda)\varepsilon_{BB}(\lambda)L_{BB}(\lambda, T_{BB}) - \rho_s(\lambda, T_{sur})R(\lambda)\varepsilon_{sur}(\lambda, T_{sur})L_{sur}(\lambda, T_{sur})}{R(\lambda)L_s(\lambda, T_s)} \quad (5)$$

Furthermore, to evaluate the thermal radiative properties of our samples, we computed the total hemispherical emissivity $\epsilon^{\cap}(T)$ at different temperatures. This quantity represents the ratio of the total radiative power emitted by a surface to that of an ideal blackbody at the same temperature, integrated over the entire spectrum. Because our measurements provide the spectral emissivity $\epsilon(\lambda)$ as a function of wavelength and not angle, and assuming the surfaces behave as Lambertian emitters (i.e., emissivity is independent of emission angle), we applied the standard formulation where the directional dependence integrates out [25]. The total hemispherical emissivity was therefore calculated using the following expression:

$$\epsilon^{\cap}(T) = \frac{\int_{\lambda_{min}}^{\lambda_{max}} \epsilon(\lambda)L_{BB}(\lambda, T_{BB})d\lambda}{\int_{\lambda_{min}}^{\lambda_{max}} L_{BB}(\lambda, T_{BB})d\lambda} \quad (6)$$

where λ_{min} and λ_{max} correspond to the lower and upper bounds of the spectral range measured by the FTIR spectrometer. The numerator represents the radiative power emitted by the sample, and the denominator corresponds to the radiative power emitted by a blackbody. This approach allows us to derive a single emissivity value at each temperature, representative of the material's radiative behavior over the thermal IR spectrum and is commonly used when angle-resolved and spectral-resolved emissivity data is not available.

E. *Uncertainty estimation using Monte Carlo simulation*

To evaluate the uncertainty in both spectral and total hemispherical emissivity, we used a Monte Carlo approach that accounts for the combined influence of measurement and model uncertainties. This method is particularly suited to complex, nonlinear equations like those used here, where analytical error propagation falls short. The spectral emissivity $\epsilon(\lambda, T)$ was calculated using several inputs (Eq. 5), including experimental signals from the sample and blackbody reference, the known emissivity of the reference, the measured reflectivity, and Planck's law. Each input was varied randomly within realistic uncertainty bounds: 1% for FTIR signals ($S_s(\lambda, T_s)$, $S_{BB}(\lambda, T_{BB})$, ρ_s), 5% for the reference emissivity (ϵ_{BB} measured indirectly), and

±5 °C for sample temperature (which affects the Planck spectral radiance calculation). For each temperature, 10,000 simulations were run to generate perturbed emissivity curves, which were then integrated using the Planck-weighted method to obtain a distribution of total emissivity values. The uncertainty was taken as the standard deviation of this distribution, offering a robust, physically consistent estimate that reflects all major sources of experimental variability. A detailed breakdown of the input parameters used in the Monte Carlo uncertainty analysis, including their uncertainty bounds and qualitative impact on the spectral emissivity calculation, is provided in the Supplementary Information (Tables S1 and S2).

III. Results and discussion

In this section, we present and analyze the results of the spectral emissivity measurements carried out on both flat and microstructured silicon samples. The goal is to assess the influence of temperature, surface structuring, and doping on their radiative behavior across the near- to mid-infrared range. The following figures highlight the evolution of emissivity with temperature, comparison with reference materials, and correlation with absorptivity at room temperature. All measurements were performed under normal incidence, and uncertainties were estimated using a Monte Carlo approach (as described in Material and Methods).

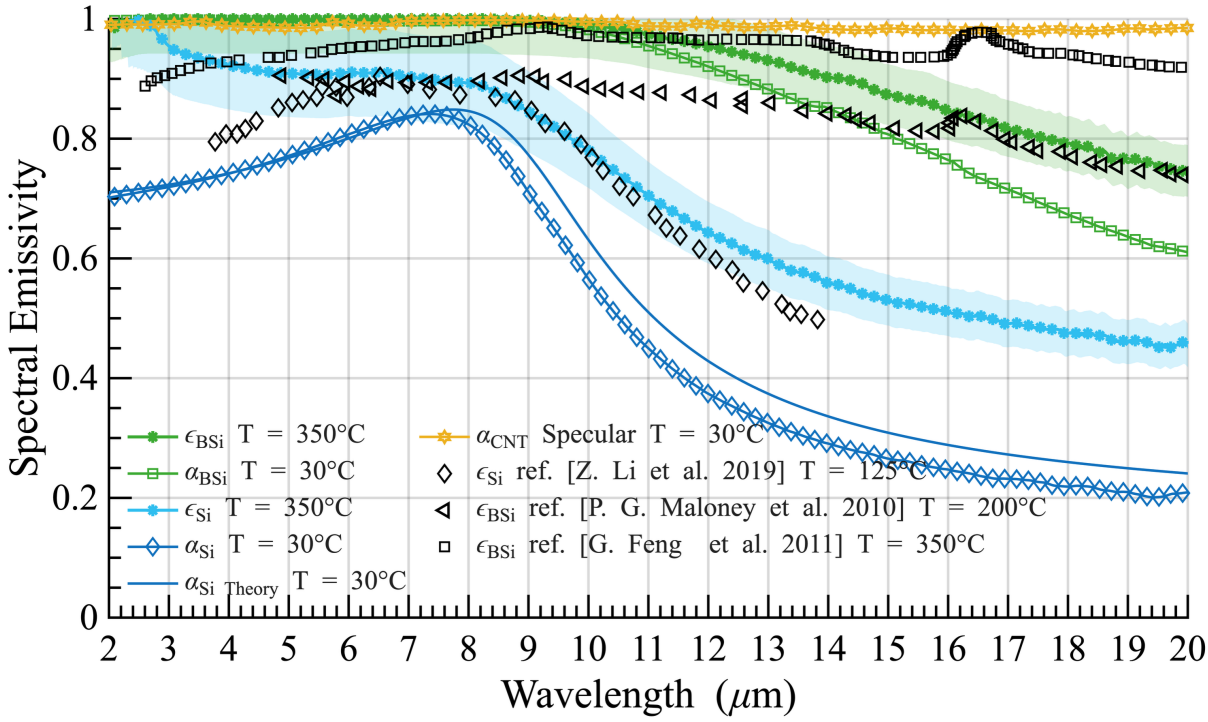

Figure 3: Spectral normal emissivities measured for both BSi (green stars) and flat Si (blue stars) at 350°C are compared to the corresponding indirect values of their normal spectral absorptivity. The solid blue line represents the theoretical simulation of the spectral absorptivity of silicon with a resistivity of 0.001 Ω·cm. The orange hexagon marks indicate the spectral absorptivity of the highly emissive CNT blackbody reference sample obtained with the indirect method. The measured emissivities are compared to

reference data from Zhe Li *et al.* [43] (black diamonds, HD Si), P.G. Maloney *et al.* [26] (black triangles, HD BSi), and G. Feng *et al.* [27] (black squares, LD BSi). The shaded areas represent the uncertainty range for each sample at this temperature, as calculated using the Monte Carlo model.

We show in Figure 3 a comparison between the measured normal absorptivity (indirect) at 30°C and the directly measured normal emissivity at 350 °C for both flat Si and BSi. It also includes the numerically computed absorptivity of the HD Si sample and the room-temperature absorptivity of the CNT BB reference sample. As shown in Figure 3, the CNT sample (orange hexagon) exhibits the expected behavior of a near-blackbody, with a spectrally flat absorptivity of approximately 0.98. This high and spectrally flat absorptivity supports the validity of using CNTs as a BB reference for direct emissivity measurements. The reliability of the setup is further confirmed by the close match between the experimental absorptivity values (blue diamonds) and theoretical predictions (blue solid line), as well as by the agreement between our direct emissivity measurements of HD flat Si (resistivity = 0.001 Ω·cm) and the reference data reported in the literature [43].

When comparing our HD BSi results (green stars) to the HD BSi data reported by G. Feng *et al.* [27] (black squares) and P. G. Maloney *et al.* [26] (black triangles), a clear difference is observed. These discrepancies can be attributed to two key factors, the doping level of the silicon substrate and the height of the microstructures. It is also important to highlight that the fabrication techniques differ across the studies. In our case, BSi was fabricated using Cryo-DRIE, whereas the other two studies employed femtosecond laser irradiation in SF_6 or Cl_2 atmospheres. In our study, the BSi features 5 µm-deep structures, while the reported structures in the comparison studies range from 10 to 30 µm. Both doping concentration and structural depth in addition to more subtle morphological features have been previously identified as key parameters for enhancing BSi absorptivity [11, 12]. Consequently, our HD BSi samples exhibit higher emissivity, approaching unity for wavelengths below 10 µm.

Furthermore, the spectral trends observed using both direct and indirect methods are consistent across the wavelength range. As expected, the emissivity of both BSi and flat Si increases with temperature [31, 32, 38]. The shaded areas in Figure 3 represent the uncertainty range for each sample at 350 °C, as estimated using the Monte Carlo model. Notably, the uncertainty on the measured emissivity decreases with increasing temperature. For BSi, the uncertainty drops from 6.01% at 150 °C to 5.79% at 350 °C, while for flat Si it decreases from 9.37% to 8.02% over the same range. The lower signal-to-noise ratio at 150 °C explains the increased noise in emissivity values observed at this temperature.

As shown in Figure 4, emissivity slightly increases with temperature while maintaining the same overall spectral trends. For clarity, uncertainty ranges are not displayed in this figure; a version including

shaded uncertainty bounds is provided in Figure S3 of the Supplementary Information. Quantitatively, we note a 120% and 30% increase in emissivity at 20 μm for HD flat Si and HD BSi, respectively, between 150 and 350 °C. Additionally, the emissivity of HD flat Si increases sharply from 0.7 to nearly unity at 2.5 μm. In all cases, BSi consistently exhibits higher emissivity than flat Si across the entire measured temperature range, reaffirming its promise for high-temperature applications such as thermal IR emitters or thermophotovoltaic selective surfaces.

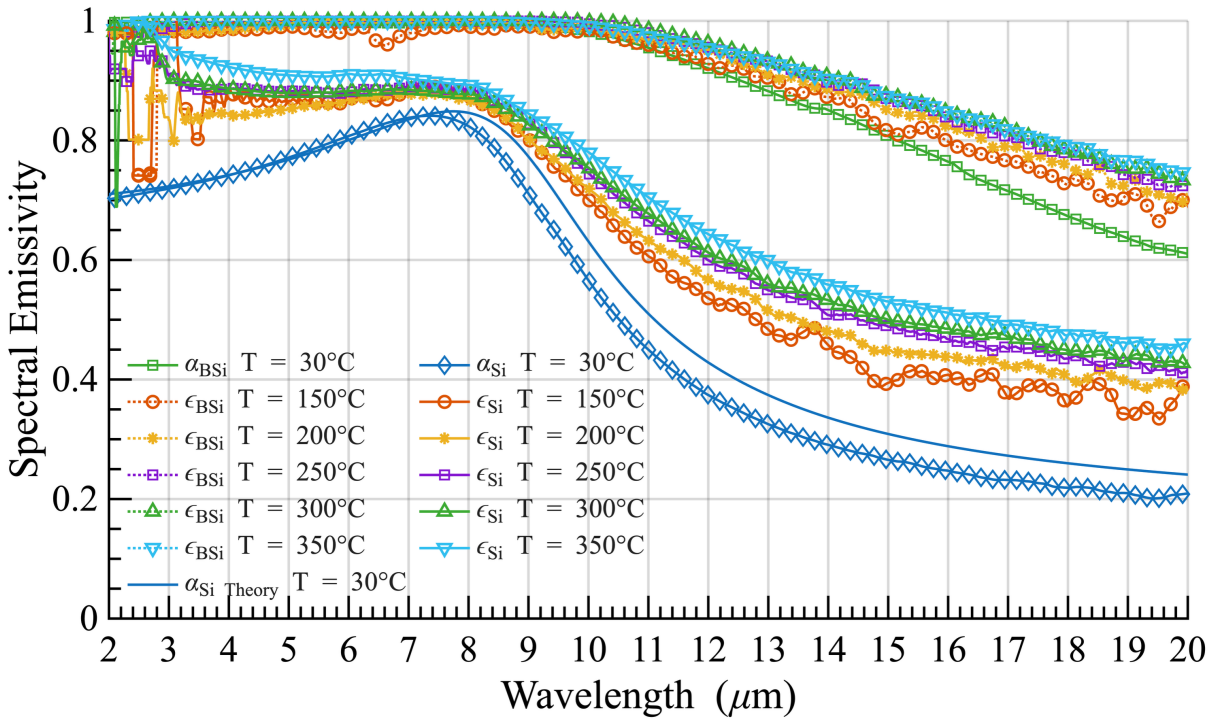

Figure 4: Spectral emissivities measured for both BSi and flat Si at different temperatures and compared to the corresponding indirect values of their spectral absorptivity. The solid blue line represents the theoretical simulation of the spectral absorptivity of silicon with a resistivity of 0.001 Ω·cm.

Furthermore, the total hemispherical emissivities versus temperature, calculated using Equation 6, are plotted in Figure 5. In both cases, emissivity increases with temperature, a trend also reported in other studies on microstructured silicon [26, 31, 33, 37]. The results for flat Si are compared with reference data from P. J. Timans [32] for HD Si (resistivity = 0.012 Ω·cm), based on earlier calculations by T. Sato [31]. Interestingly, Timans' data indicate that emissivity remains nearly constant with temperature for HD Si, while it increases sharply for LD Si. In contrast, our measurements show a moderate but clear increase in emissivity with temperature for HD Si, which diverges from Timans' findings. This discrepancy likely due from differences in the spectral integration range, but not exclusively. Indeed, theoretical studies on temperature-dependent absorption indicate that the underlying mechanisms differ significantly at high doping levels, which further

contributes to the observed variations [44]. Timans evaluated emissivity based on absorption measurements between 1.1 and 1.6 μm for temperatures up to 800 °C, whereas our study integrates over a much broader spectral range, from 2 to 20 μm. For HD BSi, the increase is more limited, unsurprising given its already high emissivity at low temperatures, nearing the physical upper limit of unity.

Additionally, our BSi results are compared with the total hemispherical emissivity data for 30 μm-deep HD BSi and 8 μm-deep LD BSi reported by P.G. Maloney *et al*. [26] and G. Feng *et al.* [27], respectively. While a similar temperature-dependent trend is observed with the results of G. Feng *et al*., the BSi fabricated in our study consistently exhibits higher emissivity values. This difference is attributed to a combination of factors, notably the morphology of the microstructures and the doping concentration. As shown experimentally and numerically by Sarkar *et al.* [11, 12], the depth and shape of conical nanostructures in BSi play a central role in achieving ultra-broadband, near-unity absorption and, by Kirchhoff's law, high emissivity. They report that increasing the structure depth up to ~10.3 μm with a high aspect ratio (up to 30:1), combined with high phosphorous doping (~5×10^{19} cm^{-3}), results in absorptance >99.5% up to 8 μm and >90% up to 20 μm. These performance levels were linked to both the suppression of transmittance due to high doping and wafer thickness, and to the tapered geometry that minimizes reflectance through impedance matching. In our study, the BSi structures were ~5 μm deep with similar doping levels (~5×10^{19} cm^{-3}), optimized for mid-IR operation. The enhanced emissivity observed compared to previous works likely arises from this specific combination of moderate structural depth, which remains sufficient to suppress reflection in the mid-IR, and high doping, which ensures minimal transmission and efficient volumetric absorption. This synergy explains the consistently higher emissivity observed in our samples, confirming the critical influence of both microstructure geometry and carrier concentration, as also discussed by Zhe Li *et al.* [43] and Sopori *et al.* [45].

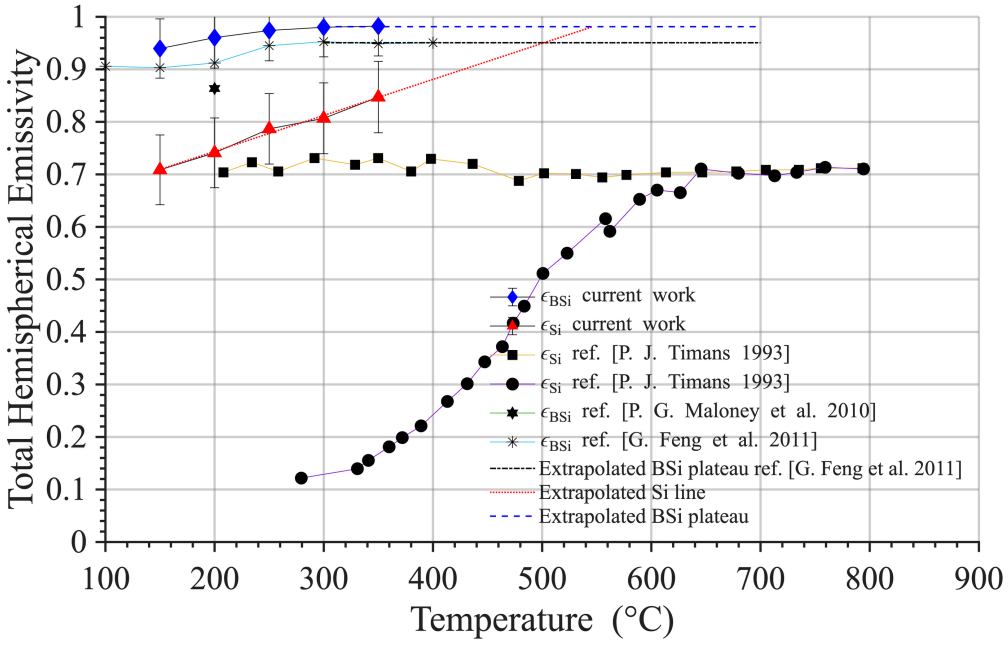

Figure 5: Total hemispherical emissivity calculated using Equation 6 for both BSi (blue diamond) and flat Si (red triangle) as a function of temperature. Si results are compared to LD (black circle resistivity = 78 Ω·cm) and HD (black square resistivity = 0.012 Ω·cm) Si reference samples from the study by P. J. Timas (1993) [32], based on the calculated values from T. Sato (1967) [31]. BSi results are compared to LD BSi reference samples from the studies of G. Feng *et al.* [27] (black stars) and P. G. Maloney *et al.* [26] (black hexagram).

Over the temperature range studied, total emissivity is strongly influenced by the spectral emissivity behavior in the 2–20 μm wavelength range, where optical absorption occurs via interactions between photons and either free carriers or lattice vibrations. At low temperatures, the concentration of free carriers is mainly determined by the doping level and is very low in lightly doped silicon [32, 43]. Consequently, free-carrier absorption is minimal, and the total emissivity is dominated by a weak contribution of the lattice vibrations, resulting in low total emissivity. As temperature increases, the thermally generated free carriers significantly enhance absorption, leading to a sharp rise in total emissivity. In contrast, heavily doped silicon already has a high carrier concentration at room temperature, and additional thermal excitation has little effect on its emissivity, resulting in a relatively stable behavior across the temperature range. This enhancement is not solely attributed to free-carrier absorption in the silicon volume but can also be linked to the excitation of surface plasmon polaritons (SPPs) at the silicon–air interface. It is important to note that the samples measured in this study are even more heavily doped than those investigated by P. J. Timas [32].

Consequently, in the case of BSi, its nanostructured surface geometry combined with high doping levels enhances light absorption through multiple scattering and light-trapping effects, resulting in

significantly higher emissivity compared to flat Si. The complex surface morphology also supports strong near-field interactions and localized electromagnetic modes, which, under specific conditions, can couple to SPPs in the mid-infrared range. This coupling further boosts spectral absorptivity and emissivity, particularly in the infrared region relevant for thermal applications. As a result, BSi exhibits a very high emissivity even at lower temperatures, which inherently limits the magnitude of any further increase with temperature, since emissivity cannot exceed unity.

Nonetheless, a slight increase in total emissivity with temperature is observed. This can be attributed to two physical mechanisms: (i) as temperature increases, the spectral range of thermal emission shifts toward shorter wavelengths according to Planck's law, activating regions where the BSi absorption may still be slightly sub-unity at lower temperatures, and (ii) temperature-induced changes in free carrier concentration and phonon interactions in heavily doped silicon can further reduce reflectivity and enhance absorption. These effects collectively explain the modest temperature-driven increase in emissivity observed in our experiments.

Furthermore, because BSi already absorbs efficiently across the relevant thermal spectral window, increases in temperature contribute only marginally to total emissivity. These combined effects explain the near-saturation of emissivity at elevated temperatures and support the use of BSi in applications requiring broadband, high-temperature radiative performance.

Moreover, as shown in Figure 5, the total hemispherical emissivity curves reported by P.J. Timans [32] reveal that, beyond a threshold temperature of approximately 650 °C, flat silicon reaches a plateau in emissivity, regardless of the doping level. A similar plateau behavior is observed for highly doped BSi. In both our work (blue dashed line) and that of G. Feng *et al.* [27] (black dash-dotted line) the plateau begins as early as 300 °C. This early stabilization of emissivity in BSi further highlights its superior radiative performance at intermediate temperatures. Interestingly, extrapolating our results (blue dashed and red dotted lines) suggests that the emissivity of HD flat Si and HD BSi could converge around 545 °C. This convergence may indicate that, at sufficiently high temperatures, emissivity becomes less sensitive to surface structuration. While speculative, this observation warrants further investigation and will be the focus of future work.

IV. Conclusions

Accurate characterization of emissivity at functional operating temperatures is essential for assessing the suitability of emerging thermal metamaterials in applications such as heat sensing, thermal management, and energy conversion, especially in intermediate to high temperature regimes. In this work, we developed a

dedicated experimental setup capable of performing direct spectral normal emissivity measurements from 150 °C to 350 °C, over a broad spectral range from 2 to 20 μm.

We report the temperature dependence of both spectral and total emissivity of BSi. The results demonstrate that BSi retains its extremely high broadband emissivity with temperature. For instance, the total hemispherical emissivity increases slightly from approximately 0.95 at 150 °C to around 0.98 at 350 °C. This limited increase is expected, as our BSi already exhibits near-unity emissivity at lower temperatures, due to its optimized microstructure and high doping level. These findings confirm BSi's excellent potential for integration into high-temperature radiative applications such as TPV emitters, thermal infrared light sources, and radiative cooling systems. In comparison, measurements on highly doped flat Si, which show good agreement with literature data, primarily serve to validate the experimental approach and support the robustness of the setup.

The results reported in this study initiate the development and deployment of BSi-based materials in advanced thermal technologies operating at elevated temperatures.

Acknowledgments

This work was supported by the I-SITE FUTURE Initiative (reference ANR-16-IDEX-0 0 03) in the framework of the projects CATBSI and METAHEAT. The authors wish to extend also their acknowledgements to the French Research Group NAME and to the National Natural Science Foundation of China (grant nos. 62134009,62121005). The authors would like also to thanks Prof Wei Li from CIOMP for valuable discussion on the direct emissivity measurements.

Data Availability The datasets generated and/or analyzed during the current study are available from the corresponding author on request.

Author Contributions

G.H, E.N., A.H. & E.A. conceived the direct emissivity setup with support from Y.A., & T.B. who made preliminary trials, A.H., G.H, E.A, & A.F. performed the experimental direct and indirect measurements and the modelling, A.D. & E.N. helped improving the emissivity setup, F.M. fabricated the silicon-based samples and did the SEM images, J.Z. fabricated the CNT-based reference blackbody samples, G.H. wrote the manuscript, G.H., A.H., E.A., E.N., A.D. & Y.A., analyzed the data and discussed the results, edited and improved the manuscript with the help of T.B. & P.B. All authors approved the last version of the manuscript.

Additional Information

Competing Interests: The authors declare that they have no competing interests.

Declaration of generative AI and AI-assisted technologies in the writing process

During the preparation of this work the authors used ChatGPT in order to improve the language and readability of this manuscript. After using this tool/service, the authors reviewed and edited the content as needed and take full responsibility for the content of the publication.

References

1. Zhang Y, Heo YJ, Son YR, et al (2019) Recent advanced thermal interfacial materials: A review of conducting mechanisms and parameters of carbon materials. Carbon 142:445–460. https://doi.org/10.1016/j.carbon.2018.10.077

2. Zhao B, Hu M, Ao X, et al (2019) Radiative cooling: A review of fundamentals, materials, applications, and prospects. Applied Energy 236:489–513. https://doi.org/10.1016/j.apenergy.2018.12.018

3. Zalba B, Marín JM, Cabeza LF, Mehling H (2003) Review on thermal energy storage with phase change: materials, heat transfer analysis and applications. Applied Thermal Engineering 23:251–283. https://doi.org/10.1016/S1359-4311(02)00192-8

4. Fan S, Li W (2022) Photonics and thermodynamics concepts in radiative cooling. Nature Photonics 16:182–190. https://doi.org/10.1038/s41566-021-00921-9

5. Xie F, Jin W, Nolen JR, et al (2024) Subambient daytime radiative cooling of vertical surfaces. Science 386:788–794. https://doi.org/10.1126/science.adn2524

6. Chai JY-H, Wong BT, Juodkazis S (2020) Black-silicon-assisted photovoltaic cells for better conversion efficiencies: a review on recent research and development efforts. Materials Today Energy 18:100539. https://doi.org/10.1016/j.mtener.2020.100539

7. Behera AK, Viswanath RN, Lakshmanan C, et al (2020) Synthesis of silicon nanowalls exhibiting excellent antireflectivity and near super-hydrophobicity. Nano-Structures & Nano-Objects 21:100424. https://doi.org/10.1016/j.nanoso.2020.100424

8. Algasinger M, Paye J, Werner F, et al (2013) Improved black silicon for photovoltaic applications. Advanced Energy Materials 3:1068–1074. https://doi.org/10.1002/aenm.201201038

9. Soueiti J, Sarieddine R, Kadiri H, et al (2023) A review of cost-effective black silicon fabrication techniques and applications. Nanoscale. https://doi.org/10.1039/d2nr06087f

10. Liu X, Coxon PR, Peters M, et al (2014) Black silicon: fabrication methods, properties and solar energy applications. Energy & Environmental Science 7:3223–3263

11. Sarkar S, Nefzaoui E, Hamaoui G, et al (2022) Wideband mid infrared absorber using surface doped black silicon. Applied Physics Letters 121:231703. https://doi.org/10.1063/5.0117289

12. Sarkar S, Elsayed AA, Sabry YM, et al (2023) Black Silicon Revisited as an Ultrabroadband Perfect Infrared Absorber over 20 μm Wavelength Range. Advanced Photonics Research 4:2200223. https://doi.org/10.1002/adpr.202200223

13. Nguyen KN, Basset P, Marty F, et al (2013) On the optical and morphological properties of microstructured Black Silicon obtained by cryogenic-enhanced plasma reactive ion etching. Journal of Applied Physics 113:194903. https://doi.org/10.1063/1.4805024

14. Saeed A, Elsayed AA, Marty F, et al (2020) Mid-infrared radiation source for spectroscopic applications based on multi-walled carbon nanotubes on top of silicon. In: Nanophotonics VIII. SPIE, pp 105–110

15. Saab DA, Mostarshedi S, Basset P, et al (2014) Effect of black silicon disordered structures distribution on its wideband reduced reflectance. Mater Res Express 1:045045. https://doi.org/10.1088/2053-1591/1/4/045045

16. Abi Saab D, Basset P, Pierotti MJ, et al (2014) Static and Dynamic Aspects of Black Silicon Formation. Phys Rev Lett 113:265502. https://doi.org/10.1103/PhysRevLett.113.265502

17. Gao L, Nefzaoui E, Marty F, et al (2022) Two-dimensional metamaterials as meta-foams for optimized surface-enhanced solar steam generation. Solar Energy Materials and Solar Cells 243:111793

18. Hervé A, Hamaoui G, Bourouina T, et al (2023) Passive Nighttime Radiative Cooling Using Black Silicon. Thessaloniki, Greece

19. Lavielle N, Othman AM, Hervé A, et al (2024) Infrared Spectral Emissivity Dynamics of Surfaces Under Water Condensation. Advanced Functional Materials 34:2403316. https://doi.org/10.1002/adfm.202403316

20. Zhu C, Hobbs MJ, Willmott JR (2020) An accurate instrument for emissivity measurements by direct and indirect methods. Measurement Science and Technology 31:. https://doi.org/10.1088/1361-6501/ab5e9b

21. MODEST Michael F. (2003) Radiative Heat Transfer Second Edition. Academic Press

22. Guo YM, Pang SJ, Luo ZJ, et al (2019) Measurement of Directional Spectral Emissivity at High Temperatures. International Journal of Thermophysics 40:. https://doi.org/10.1007/s10765-018-2472-2

23. Petra Honnerová, Jiří Martan, Martin Kučera, et al New experimental device for high-temperature normal spectral emissivity measurements of coatings. Meas Sci Technol 25:095501

24. Ji H, Liu D, Cheng H, et al (2018) Vanadium dioxide nanopowders with tunable emissivity for adaptive infrared camouflage in both thermal atmospheric windows. Solar Energy Materials and Solar Cells 175:96–101. https://doi.org/10.1016/j.solmat.2017.10.013

25. Lucchesi C, Delmas A (2023) Experimental setup for direct measurements of spectral directional emissivity from 0° to 80° angles at temperatures as low as 40 °C. International Journal of Thermal Sciences 185:. https://doi.org/10.1016/j.ijthermalsci.2022.108045

26. Maloney PG, Smith P, King V, et al (2010) Emissivity of microstructured silicon. Applied Optics 49:1065–1068. https://doi-org.univ-eiffel.idm.oclc.org/10.1364/AO.49.001065

27. Feng G, Wang Y, Li Y, et al (2011) Greatly enhanced infrared normal spectral emissivity of microstructured silicon using a femtosecond laser. Materials Letters 65:1238–1240. https://doi.org/10.1016/j.matlet.2011.01.067

28. Gengenbach J, Kabelac S, Koirala LR (2005) Measurement of directional spectral emissivities of microstructured surfaces. In: 17th European Conference on Thermophysical Properties (ECTP). Bratislava

29. Ravindra NM, Abedrabbo S, Chen W, et al (1998) Temperature-dependent emissivity of silicon-related materials and structures. IEEE Transactions on Semiconductor Manufacturing 11:30–39. https://doi.org/10.1109/66.661282

30. Macfarlane GG, McLean TP, Quarrington JE, Roberts V (1958) Fine Structure in the Absorption-Edge Spectrum of Si. Phys Rev 111:1245–1254. https://doi.org/10.1103/PhysRev.111.1245

31. Tsutomu Sato (1967) Spectral Emissivity of Silicon. Japanese Journal of Applied Physics 6:

32. Timans PJ (1993) Emissivity of silicon at elevated temperatures. Journal of Applied Physics 74:6353–6364. https://doi.org/10.1063/1.355159

33. Rogne H, Timans PJ, Ahmed H (1996) Infrared absorption in silicon at elevated temperatures. Applied Physics Letters 69:2190–2192. https://doi.org/10.1063/1.117161

34. Jellison GE, Lowndes DH (1982) Optical absorption coefficient of silicon at 1.152 μ at elevated temperatures. Applied Physics Letters 41:594–596. https://doi.org/10.1063/1.93621

35. Sturm JC, Reaves CM (1992) Silicon temperature measurement by infrared absorption. Fundamental processes and doping effects. IEEE Trans Electron Devices 39:81–88. https://doi.org/10.1109/16.108215

36. Vandenabeele P, Maex K (1992) Influence of temperature and backside roughness on the emissivity of Si wafers during rapid thermal processing. Journal of Applied Physics 72:5867–5875. https://doi.org/10.1063/1.351892

37. Ravindra NM, Sopori B, Gokce OH, et al (2001) Emissivity measurements and modeling of silicon-related materials: An overview. International Journal of Thermophysics 22:1593–1611. https://doi.org/10.1023/A:1012869710173

38. Constancio Jr M, Adhikari RX, Aguiar OD, et al (2020) Silicon emissivity as a function of temperature. International Journal of Heat and Mass Transfer 157:119863. https://doi.org/10.1016/j.ijheatmasstransfer.2020.119863

39. Jin Y, Zhang T, Huang Z, et al (2020) Broadband omnidirectional perfect absorber based on carbon nanotube films. Carbon 161:510–516. https://doi.org/10.1016/j.carbon.2020.01.106

40. Shimizu Y, Ishii J (2014) Blackbody thermal radiator with vertically aligned carbon nanotube coating. Jpn J Appl Phys 53:068004. https://doi.org/10.7567/JJAP.53.068004

41. Zhang K, Chen G, Zhou S, et al (2023) Carbon nanotube electron blackbody and its radiation spectra. Proc Natl Acad Sci USA 120:e2209670120. https://doi.org/10.1073/pnas.2209670120

42. Mauron Ph, Emmenegger Ch, Züttel A, et al (2002) Synthesis of oriented nanotube films by chemical vapor deposition. Carbon 40:1339–1344. https://doi.org/10.1016/S0008-6223(01)00295-0

43. Li Z, Zhang Y, Peng H, et al (2019) Spectral narrowing of sub-bandgap absorbance and emissivity in highly doped silicon. Materials Research Express 6:. https://doi.org/10.1088/2053-1591/ab637d

44. Elsayed AA, Sabry YM, Marty F, et al (2018) Optical modeling of black silicon using an effective medium/multi-layer approach. Opt Express 26:13443. https://doi.org/10.1364/OE.26.013443

45. Sopori B, Chen W, Madjdpour J &, Ravindra NM (1999) Calculation of Emissivity of Si Wafers. Journal of Electronic Materials 28:1385–1389